Article

Journal of Intelligent Material Systems and Structures

Journal of Intelligent Material Systems and Structures
24(7) 846–854

DOI: 10.1177/1045389X12461073
jim.sagepub.com
SAGE

# Electroaeroelastic analysis of airfoil-based wind energy harvesting using piezoelectric transduction and electromagnetic induction

**Carlos De Marqui Jr[1] and Alper Erturk[2]**

**Abstract**

The concept of transforming aeroelastic vibrations into electricity for low-power generation has received growing attention in the last few years. The goal is to convert airflow energy into electricity for powering small electronic components employed in wireless applications. The potential applications for aeroelastic energy harvesting range from aircraft structures to several engineering problems involving wireless electronic components located in high wind areas. The use of a typical airfoil section is a convenient approach to create instabilities and persistent oscillations in aeroelastic energy harvesting. This article analyzes two airfoil-based aeroelastic energy harvesters using (a) piezoelectric transduction and (b) electromagnetic induction. An airfoil with two degrees of freedom is investigated by adding piezoelectric and electromagnetic couplings to the plunge degree of freedom in two separate cases. The governing dimensionless electroaeroelastic equations are given in each case with a resistive load in the electrical domain for predicting the power output at the flutter boundary. The effects of several dimensionless system parameters on the dimensionless electrical power output as well as the dimensionless linear flutter speed are investigated for piezoelectric and electromagnetic energy harvesting from airflow-induced vibrations. The simulations presented in this study can be employed for designing and optimizing airfoil-based wind energy harvesters.

**Keywords**

Energy harvesting, piezoelectric, electromagnetic, aeroelastic

## Introduction

The research field of energy harvesting has received growing attention in both academia and industry (Anton and Sodano, 2007; Beeby et al., 2006; Cook-Chennault et al., 2008) over the last decade. The motivation in this field is due to the reduced power requirement of small electronic components, such as the wireless sensor networks used in monitoring applications, with the purpose of powering such devices using the vibrational energy available in their environment. By means of self-sustained wireless electronic components that use harvested ambient energy, the maintenance requirement for periodic battery replacement and the chemical waste of conventional batteries can be minimized.

Most of the existing research under the topic of mechanical energy harvesting has focused on transforming direct vibration input into electricity by using the electromagnetic (Amirtharajah and Chandrakasan, 1998; Elvin and Elvin, 2011; Glynne-Jones et al., 2004), electrostatic (Mitcheson et al., 2004; Roundy et al., 2003; Tvedt et al., 2010) and piezoelectric (Erturk and Inman, 2009; Jeon et al., 2005; Roundy and Wright, 2004) transduction mechanisms. Another form of energy available in the vicinity of sensor nodes and remotely operating engineering systems is due to airflow. As an alternative to miniaturized windmill configurations (Myers et al., 2007; Priya et al., 2005; Rancourt et al., 2007; Xu et al., 2010), researchers have recently considered exploiting aeroelastic vibrations for converting wind energy into electricity using scalable

[1]Department of Aeronautical Engineering, Engineering School of Sao Carlos, University of Sao Paulo, Sao Carlos, SP, Brazil
[2]G. W. Woodruff School of Mechanical Engineering, Georgia Institute of Technology, Atlanta, GA, USA

**Corresponding author:**
Carlos De Marqui Jr, Department of Aeronautical Engineering, Engineering School of Sao Carlos, University of Sao Paulo, Trabalhador Sancarlense Avenue, 400, Sao Carlos, SP 13566-590, Brazil.
Email: demarqui@sc.usp.br

configurations. An early experimental effort of generating electricity from thin curved airfoils with macrofiber composite (MFC) piezoelectric structures under airflow excitation was presented by Erturk et al. (2008). For the piezoaeroelastic problem of harvesting energy from airflow excitation of a cantilevered plate with embedded piezoceramics, De Marqui et al. (2010a, 2010b) presented finite-element models based on the vortex-lattice method (De Marqui et al., 2010a) and the doublet-lattice method (De Marqui et al., 2010b) of aeroelasticity (Bisplinghoff and Ashley, 1962; Dowell et al., 1978; Fung, 1969; Hodges and Pierce, 2002). Time-domain simulations (De Marqui et al., 2010a) were given for a cantilevered plate with embedded piezoceramics for various airflow speeds below the linear flutter speed and at the flutter boundary. Frequency-domain simulations (De Marqui et al., 2010b) considering resistive and resistive-inductive circuits were also presented focusing on the linear response at the flutter boundary. Bryant and Garcia (2009a, 2009b) studied the aeroelastic energy harvesting problem for a typical section using the finite state theory of Peters et al. (1995). Erturk et al. (2010) presented an experimentally validated lumped-parameter model for a wing section (airfoil) with piezoceramics attached onto plunge stiffness members using Theodorsen's (1935) unsteady aerodynamic model. Piezoelectric power generation at the flutter boundary, including the minor shift in the linear flutter speed, has also been discussed (Erturk et al., 2010). In addition to these recent efforts, we note that the "wingmill" concept was investigated previously for rather large-scale configurations as an alternative to conventional windmills and wind turbines (Jones and Platzer, 1999; Ly and Chasteau, 1981; McKinney and DeLaurier, 1981).

As an alternative to airfoil-based and cantilevered wing-based configurations, St Clair et al. (2010) presented a design that uses a piezoelectric beam embedded within a cavity under airflow along with experimental results. Vortex-induced oscillations of piezoelectric cantilevers located behind bluff bodies were investigated by Robbins et al. (2006), Pobering et al. (2009), and Akaydin et al. (2010) through experimental and numerical simulations. Tang et al. (2009) presented a rigorous analysis of the energy transfer from the fluid to the structure for self-excited vibrations due to axial flow over a cantilever. Piezoelectric energy harvesting from limit cycle oscillations under axial flow over a cantilever beam has been recently discussed by Dunnmon et al. (2011), Kwon (2010) considered a T-shaped cantilever beam that causes vortex street formation over the cantilever in response to axial flow.

More recently, researchers have focused on nonlinear aspects (Dowell et al., 2003) of aeroelastic energy harvesting using piezoelectric transduction and airfoil configurations. Abdelkefi et al. (2011) considered nonlinear plunge and pitch stiffness components (in polynomial forms) and theoretically investigated their effects on the harvested energy and the nonlinear aeroelastic behavior. Sousa et al. (2011) considered free play nonlinearity for the pitch stiffness and experimentally validated its effect on the harvested piezoelectric energy. The case of combined nonlinearities (free play and cubic hardening stiffness) was also numerically investigated by the same authors (Sousa et al., 2011). The free play nonlinearity has been shown to reduce the cut-in speed of persistent oscillations, while the hardening stiffness of the cubic form has been observed to make the persistent oscillations bounded at acceptable amplitudes over a wide range of airflow speeds.

Very few research groups investigated electromagnetic transduction for airflow energy harvesting although electromagnetic induction can be very effective for large displacements at low frequencies (Amirtharajah and Chandrakasan, 1998; Elvin and Elvin, 2011; Glynne-Jones et al., 2004). Zhu et al. (2010) experimentally investigated an electromagnetic energy harvester that oscillates behind a bluff body, while Jung and Lee (2011) studied electromagnetic energy harvesting from wake galloping. In the present article, two airfoil-based aeroelastic energy harvesting concepts, employing piezoelectric transduction and electromagnetic induction, are analyzed based on fully coupled electroaeroelastic modeling. The electromechanical coupling (due to piezoelectric transduction and electromagnetic induction) is coupled to the plunge degree of freedom in both cases. The governing dimensionless electroaeroelastic equations are given in each case considering a resistive load in the electrical domain. The effects of several dimensionless system parameters on the dimensionless electrical power output as well as the dimensionless linear flutter speed are investigated for the linear aeroelastic problem at the flutter boundary.

## Aeroelastic typical section for wind energy harvesting

### *Conventional aeroelastic typical section*

Figure 1 shows the schematic of a linear two-degree-of-freedom (2-DOF) typical section. The plunge and pitch displacement variables are denoted by $h$ and $\alpha$, respectively. The plunge displacement is measured at the elastic axis, that is, at point $P$ (positive downward), and the pitch angle is measured about the elastic axis (positive clockwise). In addition, $b$ is the semichord of the airfoil section, $x_\alpha$ is the dimensionless chord-wise offset of the elastic axis from the centroid ($C$), $k_h$ is the stiffness per length in the plunge DOF, $k_\alpha$ is the stiffness per length in the pitch DOF, $d_h$ is the damping coefficient per length in the plunge DOF, $d_\alpha$ is the damping coefficient per length in the pitch DOF, and $U$ is the airflow speed.

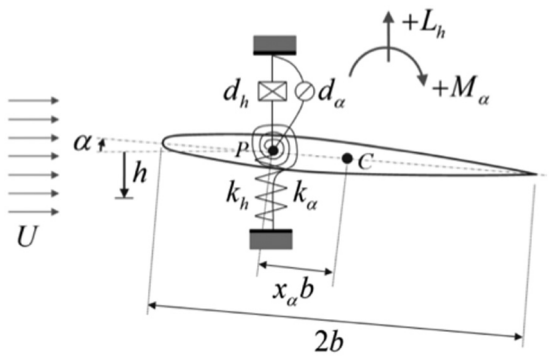


**Figure 1.** Aeroelastic typical section under airflow excitation.

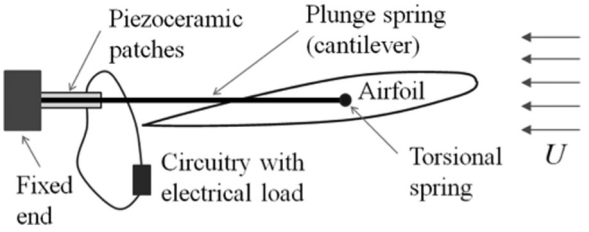


**Figure 2.** Electroaeroelastic typical section with piezoelectric coupling on the plunge DOF and an external electrical load (piezoelectric patches are attached to the plunge spring).

The governing linear aeroelastic equations are (Bisplinghoff and Ashley, 1962; Dowell et al., 1978; Fung, 1969; Hodges and Pierce, 2002)

$$(m + m_e)\ddot{h} + mbx_\alpha\ddot{\alpha} + d_h\dot{h} + k_h h = -L \tag{1}$$

$$mbx_\alpha\ddot{h} + I_\alpha\ddot{\alpha} + d_\alpha\dot{\alpha} + k_\alpha\alpha = M \tag{2}$$

where $m$ is the airfoil mass per length (in the span direction), $m_e$ is the fixture mass (connecting the airfoil to the plunge springs) per length, $M$ is the aerodynamic moment, $L$ is the aerodynamic lift, and the over-dot represents differentiation with respect to time ($t$). In the cases investigated in this study, the unsteady aerodynamic loads (lift and moment terms in equations (1) and (2)) due to arbitrary motions are obtained from Jones' (1938) approximation to Wagner's (1925) indicial function, which is equivalent to the generalized Theodorsen function (Bisplinghoff and Ashley, 1962; Theodorsen, 1935). The fixture mass ($m_e$) is defined for the case when the system slightly deviates from the ideal typical section depicted in Figure 1 due to the masses of the shaft, spring mass, and other attachments in real experiments (Sousa et al., 2011), while it is zero in the ideal representation of Figure 1.

### *Aeroelastic typical section with piezoelectric transduction*

Schematic of an electroaeroelastic section for piezoelectric energy harvesting from airflow excitation is shown in Figure 2. Aeroelastic vibrations of the cantilever (plunge spring) strain the piezoelectric patches dynamically and produces the electrical output. Therefore, piezoelectric coupling is added to the plunge DOF of the typical section, and the resultant of the electrodes is connected to a resistive load. After this modification, the linear piezoaeroelastic equations are obtained as

$$(m + m_e)\ddot{h} + mbx_\alpha\ddot{\alpha} + d_h\dot{h} + k_h h - \frac{\theta}{l}v = -L \tag{3}$$

$$mbx_\alpha\ddot{h} + I_\alpha\ddot{\alpha} + d_\alpha\dot{\alpha} + k_\alpha\alpha = M \tag{4}$$

$$C_p\dot{v} + \frac{v}{R_l} + \theta\dot{h} = 0 \tag{5}$$

where $l$ is the span length, $R_l$ is the load resistance in the electrical domain, $v$ is the voltage across the resistive load, $C_p$ is the equivalent capacitance of the piezoceramic layers, and $\theta$ is the electromechanical coupling.

Equations (3) to (5) can be written in dimensionless form as

$$\beta\bar{h}'' + x_\alpha\alpha'' + \zeta_h\bar{h}' + \bar{h} - \kappa\bar{v} = -L_h \tag{6}$$

$$x_\alpha\bar{h}'' + \bar{r}_\alpha^2\alpha'' + \zeta_\alpha\alpha' + \gamma^2\bar{r}_\alpha^2\alpha = M_\alpha \tag{7}$$

$$\eta\bar{v}' + \frac{\bar{v}}{\lambda_l} + \kappa\bar{h}' = 0 \tag{8}$$

where $\beta = (m + m_e)/m$, $\bar{h} = h/b$ is the dimensionless plunge displacement, $\zeta_h = d_h/m\omega_h$ is the plunge damping ratio, $\zeta_\alpha = d_\alpha/mb^2\omega_h$ is the pitch damping ratio, $\bar{r}_\alpha = r_\alpha/b$ is the dimensionless ratio of gyration, $\bar{v} = v/v^*$ (where $v^* = 1\,\mathrm{V}$ is the reference voltage for normalization), $\kappa = \theta v^*/lmb\omega_h^2$ is the dimensionless electromechanical coupling, $\eta = C_p v^{*^2}/mb^2l\omega_h^2$ is the dimensionless equivalent capacitance, $\lambda_l = R_l mb^2 l\omega_h^3/v^{*^2}$ is the dimensionless load resistance, $\gamma = \omega_\alpha/\omega_h$ is the frequency ratio, $\omega_h^2 = k_h/m$ is the square of the plunge natural frequency, and $\omega_\alpha^2 = k_\alpha/I_\alpha$ is the square of the pitch natural frequency. The dimensionless aerodynamic loads are $L_h = L/mb\omega_h^2$ and $M_\alpha = M/mb^2\omega_h^2$. The prime ($'$) denotes the differentiation with respect to the dimensionless time $\tau = \omega_h t$.

The piezoaeroelastic equations can be represented in the state-space form proposed (for the aeroelastic problem) by Edwards et al. (1979) by introducing the effect of electromechanical coupling. Therefore, the voltage output should be considered as an additional state variable. Two augmented aerodynamic states ($\mathbf{x}_a = \{x_1 \quad x_2\}^t$, where the superscript $t$ stands for the transpose) are included in the state-space representation of the piezoaeroelastic problem. The state-space piezoaeroelastic equations in the matrix form are

$$\begin{bmatrix} \mathbf{I} & \mathbf{0} & \mathbf{0} & 0 \\ \mathbf{0} & \tilde{\mathbf{M}} & \mathbf{0} & 0 \\ \mathbf{0} & \mathbf{0} & \mathbf{I} & 0 \\ \mathbf{0} & \mathbf{0} & \mathbf{0} & \eta \end{bmatrix} \begin{Bmatrix} \mathbf{x}' \\ \mathbf{x}'' \\ \mathbf{x}'_a \\ \bar{v}' \end{Bmatrix} = \begin{bmatrix} \mathbf{0} & \mathbf{I} & \mathbf{0} & 0 \\ -\tilde{\mathbf{K}} & -\tilde{\mathbf{B}} & \mathbf{D} & \Theta_1 \\ \mathbf{E}_1 & \mathbf{E}_2 & \mathbf{F} & 0 \\ \mathbf{0} & \Theta_2 & \mathbf{0} & \frac{1}{\lambda_l} \end{bmatrix} \begin{Bmatrix} \mathbf{x} \\ \mathbf{x}' \\ \mathbf{x}_a \\ \bar{v} \end{Bmatrix} \tag{9}$$

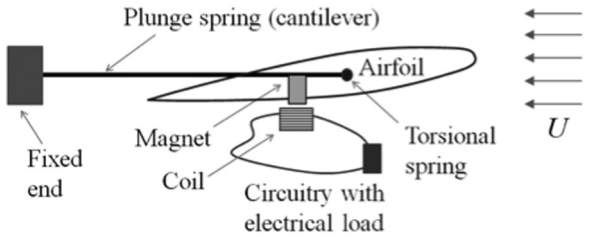


**Figure 3.** Electroaeroelastic typical section with electromagnetic coupling on the plunge DOF and an external electrical load (magnet is attached to the plunge spring).

where $\Theta_1 = \{0 \quad \kappa\}^t$, $\Theta_2 = \{0 \quad \kappa\}$, $\mathbf{x} = \{\alpha \quad \bar{h}\}^t$, and $\mathbf{I}$ is the 2×2 identity matrix. The mass, stiffness, and damping-related matrices in equation (9) are

$$\tilde{\mathbf{M}} = \mathbf{M} - \frac{\rho b^2}{m}\mathbf{M}_{nc} \tag{10}$$

$$\tilde{\mathbf{K}} = \mathbf{K} - \frac{\rho b^2}{m}\left(\frac{U}{b}\right)^2\left(\mathbf{K}_{nc} + \frac{1}{2}\mathbf{R}\mathbf{S}_1\right) \tag{11}$$

$$\tilde{\mathbf{B}} = \mathbf{B} - \frac{\rho b^2}{m}\left(\frac{U}{b}\right)\left(\mathbf{B}_{nc} + \frac{1}{2}\mathbf{R}\mathbf{S}_2\right) \tag{12}$$

where $\mathbf{M}$ is the structural mass matrix; $\mathbf{B}$ is the structural damping matrix; $\mathbf{K}$ is the structural stiffness matrix; $\rho$ is the air density; and $\mathbf{M}_{nc}$, $\mathbf{B}_{nc}$, and $\mathbf{K}_{nc}$ are noncirculatory aerodynamic matrices related to inertia, damping, and stiffness. These matrices as well as the aerodynamic matrices $\mathbf{D}$, $\mathbf{E}_1$, $\mathbf{E}_2$, $\mathbf{F}$, $\mathbf{R}$, $\mathbf{S}_1$, and $\mathbf{S}_2$ can be found in Edwards et al. (1979).

Equation (9) can be also represented as

$$\dot{\tilde{\mathbf{x}}} = \mathbf{A}\tilde{\mathbf{x}} \tag{13}$$

where

$$\mathbf{A} = \begin{bmatrix} \mathbf{0} & \mathbf{I} & \mathbf{0} & 0 \\ -\tilde{\mathbf{M}}^{-1}\tilde{\mathbf{K}} & -\tilde{\mathbf{M}}^{-1}\tilde{\mathbf{B}} & \tilde{\mathbf{M}}^{-1}\mathbf{D} & \tilde{\mathbf{M}}^{-1}\Theta_1 \\ \mathbf{E}_1 & \mathbf{E}_2 & \mathbf{F} & 0 \\ \mathbf{0} & \left(\frac{1}{\eta}\right)\Theta_2 & \mathbf{0} & \left(\frac{1}{\eta}\right)\left(\frac{1}{\lambda_l}\right) \end{bmatrix} \tag{14}$$

$$\tilde{\mathbf{x}} = \{\mathbf{x} \quad \mathbf{x}' \quad \mathbf{x}_a \quad \bar{v}\}^t \tag{15}$$

## Aeroelastic typical section with electromagnetic induction

Electromagnetic energy harvesting from airflow excitation can be realized by employing the electroaeroelastic typical section configuration as shown in Figure 3. The magnet is attached to the cantilever (plunge spring), and it oscillates relative to the coil to produce electricity in response to aeroelastic vibrations. Therefore, electromagnetic induction is added to the plunge DOF along with a resistive load in the electrical domain of the problem. The linear electromagnetically coupled electroaeroelastic equations are then

$$(m + m_e)\ddot{h} + mbx_\alpha\ddot{\alpha} + d_h\dot{h} + k_h h - \frac{B_l}{l}I = -L \tag{16}$$

$$mbx_\alpha\ddot{h} + I_\alpha\ddot{\alpha} + d_\alpha\dot{\alpha} + k_\alpha\alpha = M \tag{17}$$

$$L_c\dot{I} + (R_c + R_l)I + B_l\dot{h} = 0 \tag{18}$$

where $l$ is the span length, $R_l$ is the load resistance in the electrical domain, $R_c$ is the internal resistance of the inductor coil, $I$ is the induced electrical current, $L_c$ is the coil inductance, and $B_l$ is the electromagnetic coupling. Note that the electrical equation is kept in its general form as in Amirtharajah and Chandrakasan (1998) and Elvin and Elvin (2011) to account for the inherent coil inductance and resistance.

Equations (16) to (18) can be written in dimensionless form as

$$\beta\bar{h}'' + x_\alpha\alpha'' + \zeta_h\bar{h}' + \bar{h} - \chi\bar{I} = -L_h \tag{19}$$

$$x_\alpha\bar{h}'' + \bar{r}_\alpha^2\alpha'' + \zeta_\alpha\alpha' + \gamma^2\bar{r}_\alpha^2\alpha = M_\alpha \tag{20}$$

$$\varphi\bar{I}' + \lambda_c\bar{I} + \lambda_l\bar{I} + \chi\bar{h}' = 0 \tag{21}$$

where $\beta = (m + m_e)/m$ is the dimensionless mass ratio, $\bar{h} = h/b$ is the dimensionless plunge displacement, $\zeta_h = d_h/m\omega_h$ is the plunge damping ratio, $\zeta_\alpha = d_\alpha/mb^2\omega_h$ is the pitch damping ratio, $\bar{r}_\alpha = r_\alpha/b$ is the dimensionless ratio of gyration, $\bar{I} = I/I^*$ is the dimensionless induced current ($I^*$ is the reference current for normalization: $I^* = 1\,\mathrm{A}$ for simplicity), $\chi = B_l I^*/lmb\omega_h^2$ is the dimensionless electromagnetic coupling, $\varphi = L_c I^{*2}/lmb^2\omega_h^2$ is the dimensionless coil inductance, $\lambda_c = R_c I^{*2}/lmb^2\omega_h^3$ is the dimensionless internal resistance of the coil, $\lambda_l = R_l I^{*2}/lmb^2\omega_h^3$ is the dimensionless load resistance, $\gamma = \omega_\alpha/\omega_h$ is the frequency ratio, $\omega_h^2 = k_h/m$ is the square of the plunge natural frequency and $\omega_\alpha^2 = k_\alpha/I_\alpha$ is the square of the pitch natural frequency. As in the case of piezoelectric coupling, the dimensionless aerodynamic loads are $L_h = L/mb\omega_h^2$ and $M_\alpha = M/mb^2\omega_h^2$ while a prime ($'$) denotes differentiation with respect to the dimensionless time $\tau = \omega_h t$.

The linear equations can be represented in the state-space form by considering the dimensionless electric current ($\bar{I}$) as an additional state variable. The two augmented aerodynamic states, $\mathbf{x}_a = \{x_1 \quad x_2\}^t$, are included in the following state-space representation of the problem

$$\begin{bmatrix} \mathbf{I} & \mathbf{0} & \mathbf{0} & \mathbf{0} \\ \mathbf{0} & \tilde{\mathbf{M}} & \mathbf{0} & \mathbf{0} \\ \mathbf{0} & \mathbf{0} & \tilde{\mathbf{I}} & \mathbf{0} \\ \mathbf{0} & \mathbf{0} & \mathbf{0} & \psi \end{bmatrix}\begin{Bmatrix} \mathbf{x}' \\ \mathbf{x}'' \\ \mathbf{x}'_a \\ \bar{I}' \end{Bmatrix} = \begin{bmatrix} \mathbf{0} & \mathbf{I} & \mathbf{0} & \mathbf{0} \\ -\tilde{\mathbf{K}} & -\tilde{\mathbf{B}} & \tilde{\mathbf{D}} & \mathbf{X}_1 \\ \tilde{\mathbf{E}}_1 & \tilde{\mathbf{E}}_2 & \tilde{\mathbf{F}} & \mathbf{0} \\ \mathbf{0} & \mathbf{X}_2 & \mathbf{0} & Z \end{bmatrix}\begin{Bmatrix} \mathbf{x} \\ \mathbf{x}' \\ \mathbf{x}_a \\ \bar{I} \end{Bmatrix} \tag{22}$$

**Table 1.** Properties of the aeroelastic energy harvester.

| | |
|---|---|
| $\beta$ | 2.5940 |
| $x_\alpha$ | 0.25 |
| $\bar{r}_\alpha$ | 0.5467 |
| $\gamma$ | 0.5090 |
| $\zeta_h$ | 0.0535 |
| $\zeta_\alpha$ | 0.1102 |

where $\mathrm{X}_1 = \{0 \quad \chi\}^t$, $\mathrm{X}_2 = \{0 \quad -\chi\}$, $\mathbf{x} = \{\alpha \quad \bar{h}\}^t$, $Z = (\lambda_c + \lambda_l)$, and $\mathbf{I}$ is the 2×2 identity matrix. The mass, stiffness, and damping-related matrices are defined as in equations (10) to (12).

## Case studies

This section presents two case studies using the electro-aeroelastic models described in this article. The effects of several dimensionless system parameters on the dimensionless electrical power as well as the dimensionless linear flutter speed are investigated in the case of a typical section with piezoelectric transduction and a typical section with electromagnetic induction. In both cases, the flutter speed of each set of dimensionless parameters (electromechanical coupling, capacitance, and load resistance) is obtained by checking the real part of the eigenvalues of the state matrix with increasing airflow speed. The power output is obtained from the time histories at the flutter speed of each set of dimensionless parameters. The dimensionless properties of the typical section are shown in Table 1 (these are the fixed system parameters employed in the following simulations), and they represent the experimental setup used by Sousa et al. (2011).

### *Typical section with piezoelectric transduction*

In the first case study, the effects of dimensionless electromechanical coupling, dimensionless load resistance, and dimensionless equivalent capacitance on the dimensionless electrical power as well as the dimensionless linear flutter speed of the piezoelectrically coupled typical section are investigated. The original electroelastic parameters belong to the experimental setup used by Sousa et al. (2011), where two piezoceramics (QP10n) were added to the plunge springs of an experimental typical section. The parallel connection gives an equivalent capacitance of 120 nF (yielding $\eta = 3.66\times10^{-9}$), and the calculated electromechanical coupling is 1.55 mV/N (yielding $\kappa = 5.90\times10^{-6}$). In this case study, the simulations are performed for dimensionless parameters ranging from 0.5 to 1.5 times the original values ($\eta = 3.66\times10^{-9}$ and $\kappa = 5.90\times10^{-6}$). Also, a set of load resistance values ranging from near short-circuit (100 Ω) to open-circuit (1 MΩ) conditions is considered.

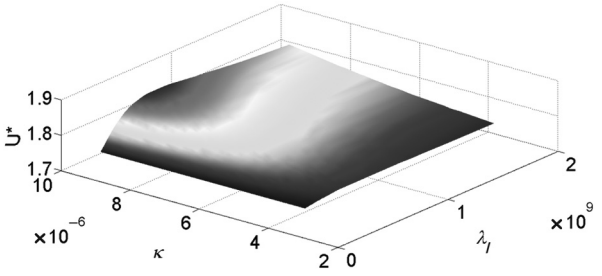


**Figure 4.** Variation of the dimensionless flutter speed with dimensionless load resistance and electromechanical coupling (for fixed dimensionless capacitance: $\eta = 3.66\times10^{-9}$).

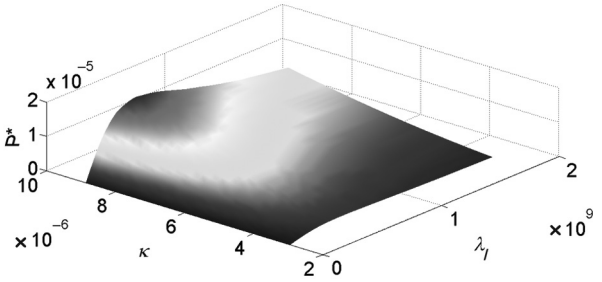


**Figure 5.** Variation of the dimensionless power output with dimensionless load resistance and electromechanical coupling (for fixed dimensionless capacitance: $\eta = 3.66\times10^{-9}$).

The variation of dimensionless flutter speed ($U^* = U/\omega_h b$) with dimensionless load resistance ($\lambda_l$) and electromechanical coupling ($\kappa$) is displayed in Figure 4 for fixed dimensionless capacitance ($\eta = 3.66\times10^{-9}$). The linear flutter speed increases with increasing dimensionless coupling for all values of load resistance. Moreover, a finite optimum load (that gives the largest flutter speed) is obtained for each dimensionless electromechanical coupling.

Figure 5 shows the variation of dimensionless electrical power output ($P^* = \bar{v}^2/\lambda_l$) with dimensionless load resistance and electromechanical coupling obtained at each dimensionless flutter speed of Figure 4 for a fixed value of dimensionless capacitance. The electrical power output increases with increasing dimensionless electromechanical coupling for any dimensionless load resistance. The presence of an optimum load resistance (that gives the maximum power output) for all values of electromechanical coupling can be observed in Figure 5. Note that the optimum load varies with changing dimensionless coupling.

Figure 6 shows the variation of dimensionless flutter speed with dimensionless load resistance and dimensionless capacitance. The value of electromechanical coupling is $\kappa = 5.90\times10^{-6}$ in this figure. The linear flutter speed decreases with increasing dimensionless capacitance for all values of load resistance (except for very low values of dimensionless load resistances).

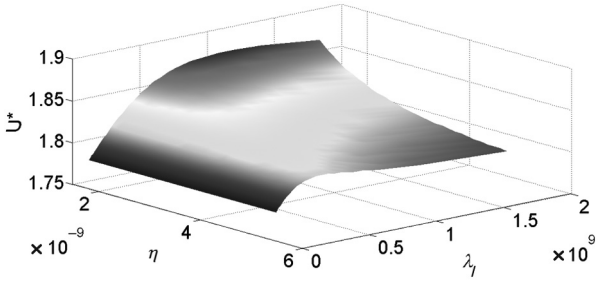


**Figure 6.** Variation of the dimensionless flutter speed with dimensionless load resistance and capacitance (for fixed dimensionless electromechanical coupling: $\kappa = 5.90\times10^{-6}$).

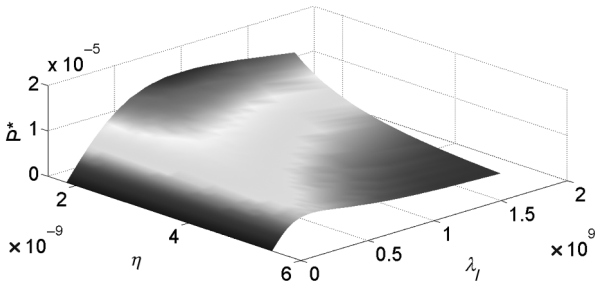


**Figure 7.** Variation of the dimensionless power output with dimensionless load resistance and equivalent capacitance (for fixed dimensionless electromechanical coupling: $\kappa = 5.90\times10^{-6}$).

Moreover, a finite optimum load that gives the largest flutter speed is obtained for each dimensionless capacitance.

Figure 7 shows the variation of dimensionless electrical power output with dimensionless load resistance and capacitance obtained at each dimensionless flutter speed of Figure 6 for fixed electromechanical coupling ($\kappa = 5.90\times10^{-6}$). The electrical power output decreases with increasing dimensionless capacitance for any dimensionless load resistance (except for very low values of dimensionless load resistance). The presence of an optimum load resistance (that gives the maximum power output) can be observed in Figure 7 for all values of dimensionless capacitance. The optimum load varies with changing dimensionless capacitance.

### *Typical section with electromagnetic induction*

In the second case study, the effects of dimensionless electromechanical coupling, dimensionless load resistance, and dimensionless coil inductance on the dimensionless electrical power as well as the dimensionless linear flutter speed are investigated. The dimensionless properties of the typical section (fixed system parameters) are shown in Table 1. A coil with an inductance of 428 mH (yielding $\varphi = 0.0130$) and internal resistance of 175 Ω (yielding $\lambda_c = 0.1022$) is considered. The magnets are attached to the plunge springs, and the dimensionless electromechanical coupling is $\chi = 0.0457$. In this case study, the simulations are performed for dimensionless parameters ranging from 0.5 to 1.5 of the original values ($\varphi = 0.0130$ and $\chi = 0.0457$), while the dimensionless load resistance range covers interval of short-circuit to open-circuit conditions.

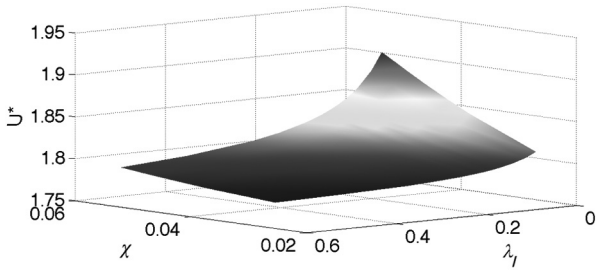


**Figure 8.** Variation of the dimensionless flutter speed with dimensionless load resistance and electromechanical coupling (for fixed dimensionless coil inductance: $\varphi = 0.0130$).

The variation of dimensionless flutter speed with dimensionless load resistance and electromechanical coupling is displayed in Figure 8. The linear flutter speed increases with increasing dimensionless coupling for all values of load resistance. Moreover, the flutter speed decreases with increasing load resistance for any dimensionless coupling (since the short-circuit stiffness is larger than the open-circuit stiffness due to electromagnetic coupling in the presence of finite coil inductance (Amirtharajah and Chandrakasan, 1998; Elvin and Elvin, 2011), and this is the opposite of the piezoelectric transduction case (De Marqui et al., 2010a; Erturk and Inman, 2009)). Note that the dimensionless coil inductance used in Figure 8 is $\varphi = 0.0130$. Further simulations (not shown here) reveal that the variation of the flutter speed depends on the presence of internal coil resistance. For instance, when the internal coil resistance is neglected ($\lambda_c = 0$) in this particular case study, a finite and nonzero optimum load that gives the largest flutter speed is obtained, analogous to the piezoelectric coupling case.

Figure 9 shows the variation of dimensionless electrical power output ($P^* = \bar{I}^2\lambda_l$) with dimensionless load resistance and electromechanical coupling obtained at each dimensionless flutter speed of Figure 8 (note that the dimensionless load axis in Figure 8 is reversed for clarity). The electrical power output increases with increasing dimensionless electromechanical coupling for any dimensionless load resistance. The presence of an optimum load resistance (that gives the maximum power output) for all values of electromechanical coupling can be observed in Figure 9. The optimum load slightly varies with changing dimensionless coupling. The optimum value of $\lambda_l$ is close to $\lambda_c$ for the range of

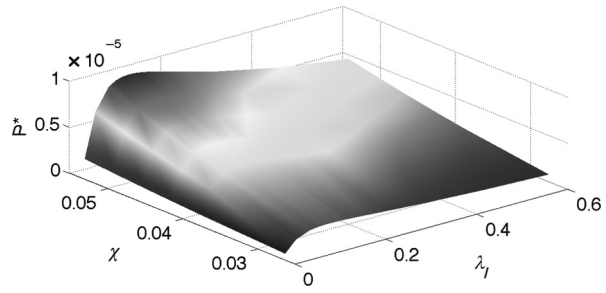


**Figure 9.** Variation of the dimensionless power output with dimensionless load resistance and electromechanical coupling (for fixed dimensionless coil inductance: $\varphi = 0.0130$).

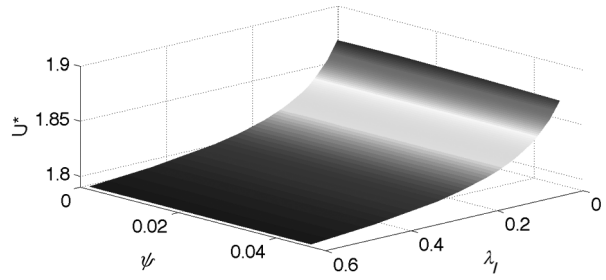


**Figure 10.** Variation of the dimensionless flutter speed with dimensionless load resistance and coil inductance (for fixed dimensionless electromechanical coupling: $\chi = 0.0457$).

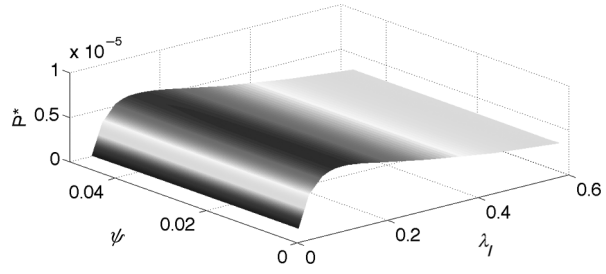


**Figure 11.** Variation of the dimensionless power output with dimensionless load resistance and coil inductance (for fixed dimensionless electromechanical coupling: $\chi = 0.0457$).

dimensionless coupling values considered. That is, the optimal load resistance of the maximum power is around the internal resistance in agreement with the maximum power transfer theorem (Agarwal and Lang, 2005).

Figure 10 shows the variation of dimensionless flutter speed with dimensionless load resistance and coil inductance. The value of electromechanical coupling is $\chi = 0.0457$ in this figure. The flutter speed decreases with increasing load resistance, as discussed with Figure 8. The dimensionless flutter speed does not change significantly with dimensionless inductance for any value of load resistance. The last simulation (Figure 11) of the linear configuration displays the variation of the dimensionless power output with dimensionless load resistance and coil inductance for each flutter speed of Figure 10. As in the case of flutter speed, the electrical power output is insensitive to the dimensionless inductance. An optimum load that gives maximum power output is obtained at each inductance level, and this optimum load slightly varies with changing dimensionless inductance.

## Conclusion

Airfoil-based aeroelastic energy harvester configurations using piezoelectric transduction and electromagnetic induction are modeled and analyzed. A two-dimensional airfoil with plunge and pitch DOF is considered by adding piezoelectric and electromagnetic couplings to the plunge DOF in two separate cases. The governing dimensionless electroaeroelastic equations are given in each case with a resistive load in the electrical domain. The effects of dimensionless system parameters on the electroaeroelastic behavior (dimensionless electrical power output and dimensionless linear flutter speed) of each harvester are discussed. In the first case (piezoelectric transduction), the optimal values of load resistance that give the largest flutter speed, as well as the maximum power output, are obtained for the range of dimensionless equivalent capacitance and dimensionless electromechanical coupling. In the second case (electromagnetic induction), the electroaeroelastic behavior of the harvester is shown to be strongly dependent on the presence of the internal coil resistance. The dimensionless flutter speed decreases with increasing load resistance for any dimensionless inductance or electromechanical coupling. Although not shown in this article, when the internal coil resistance is neglected, a finite optimum load resistance of the maximum flutter speed is obtained. Optimal values of load resistance that give the maximum power output are obtained for the range of dimensionless inductance and dimensionless electromechanical coupling considered in this study. In all cases, it is observed that the maximum power is obtained for an electrical load around the internal coil resistance in agreement with the maximum power transfer theorem.

### Funding

This study was partially funded by CNPq and FAPEMIG through the INCT-EIE and by CNPq under grant numbers 558646/2010-7 and 484132/2010-5.

### References

Abdelkefi A, Nayfeh AH and Hajj MR (2011) Modeling and analysis of piezoaeroelastic energy harvesters. *Nonlinear Dynamics*. Epub ahead of print 21 April 2011. DOI: 10.1007/s11071-011-0035-1.

Agarwal A and Lang J (2005) *Foundations of Analog and Digital Electronic Circuits*. San Francisco, CA: Morgan Kaufmann Publishers (Elsevier).

Akaydin HD, Elvin N and Andreopoulos Y (2010) Wake of a cylinder: a paradigm for energy harvesting with piezoelectric materials. *Experiments in Fluids* 49: 291–304.

Amirtharajah R and Chandrakasan AP (1998) Self-powered signal processing using vibration-based power generation. *IEEE Journal of Solid-State Circuits* 33: 687–695.

Anton SR and Sodano HA (2007) A review of power harvesting using piezoelectric materials (2003–2006). *Smart Materials and Structures* 16: R1–R21.

Beeby SP, Tudor MJ and White NM (2006) Energy harvesting vibration sources for microsystems applications. *Measurement Science & Technology* 17: R175–R195.

Bisplinghoff RL and Ashley H (1962) *Principles of Aeroelasticity*. New York: John Wiley & Sons.

Bryant M and Garcia E (2009a) Development of an aeroelastic vibration power harvester. In: *Proceedings of SPIE conference on Active and Passive Smart Structures and Integrated Systems*, San Diego, CA, 9 March 2009, vol. 7288, p. 728812.

Bryant M and Garcia E (2009b) Energy harvesting: a key to wireless sensor nodes. In: *Proceedings of SPIE Second International Conference on Smart Materials and Nanotechnology Engineering*, Weihai, China, 8 July 2009, vol. 7493, p. 74931W.

Cook-Chennault KA, Thambi N and Sastry AM (2008) Powering MEMS portable devices—a review of non-regenerative and regenerative power supply systems with emphasis on piezoelectric energy harvesting systems. *Smart Materials and Structures* 17: 043001 (33 pp.).

De Marqui C Jr, Erturk A and Inman DJ (2010a) Piezoaeroelastic modeling and analysis of a generator wing with continuous and segmented electrodes. *Journal of Intelligent Material Systems and Structures* 21: 983–993.

De Marqui C Jr, Vieira WGR, Erturk A, et al. (2010b) Modeling and analysis of piezoelectric energy harvesting from aeroelastic vibrations using the doublet-lattice method. *Journal of Vibration and Acoustics: Transactions of the ASME* 133: 011003.

Dowell EH, Curtiss HC Jr, Scalan RH, et al. (1978) *A Modern Course in Aeroelasticity*. Sijthoff and Norrdhoff: The Hagues.

Dowell EH, Edwards J and Strganac T (2003) Nonlinear aeroelasticity. *Journal of Aircraft* 40: 857–874.

Dunnmon JA, Stanton SC, Mann BP, et al. (2011) Power extraction from aeroelastic limit cycle oscillations. *Journal of Fluids and Structures* 27: 1182–1198.

Edwards JW, Ashley H and Breakwell JV (1979) Unsteady aerodynamic modeling for arbitrary motions. *AIAA Journal* 17(4): 365–374.

Elvin N and Elvin A (2011) An experimentally validated electromagnetic energy harvesters. *Journal of Sound and Vibration* 330: 2314–2324.

Erturk A and Inman DJ (2009) An experimentally validated bimorph cantilever model for piezoelectric energy harvesting from base excitations. *Smart Materials and Structures* 18: 025009.

Erturk A, Bilgen O, Fontenille M, et al. (2008) Piezoelectric energy harvesting from macro-fiber composites with an application to morphing wing aircrafts. In: *Proceedings on the 19th international conference of adaptive structures and technologies*, Ascona, Switzerland, 6–9 October.

Erturk A, Vieira WGR, De Marqui C Jr, et al. (2010) On the energy harvesting potential of piezoaeroelastic systems. *Applied Physics Letters* 96: 184103.

Fung YC (1969) *Introduction to the Theory of Aeroelasticity*. New York: Dover Publications.

Glynne-Jones P, Tudor MJ, Beeby SP, et al. (2004) An electromagnetic, vibration-powered generator for intelligent sensor systems. *Sensors and Actuators A: Physical* 110: 344–349.

Hodges DH and Pierce GA (2002) *Introduction to Structural Dynamics and Aeroelasticity*. New York: Cambridge University Press.

Jeon YB, Sood R, Jeong JH, et al. (2005) MEMS power generator with transverse mode thin film PZT. *Sensors and Actuators A: Physical* 122: 16–22.

Jones KD and Platzer MF (1999) Oscillating-wing power generator. In: *Proceedings of ASME/JSME joint fluids engineering conference*, No. 7050.

Jones RT (1938) *Operational treatment of the non-uniform lift theory in airplane dynamics*. Technical note 667. NASA.

Jung HJ and Lee SW (2011) The experimental validation of a new energy harvesting system based on the wake galloping Phenomenon. *Smart Materials and Structures* 20: 055022.

Kwon SD (2010) A T-shaped piezoelectric cantilever for fluid energy harvesting. *Applied Physics Letters* 77: 164102.

Ly KH and Chasteau VAL (1981) Experiments on an oscillating-wing aerofoil and application to wing-energy converters. *Journal of Energy* 5: 116–121.

McKinney W and DeLaurier JD (1981) The wingmill: an oscillating-wing windmill. *Journal of Energy* 5: 109–115.

Mitcheson P, Miao P, Start B, et al. (2004) MEMS electrostatic micro-power generator for low frequency operation. *Sensors and Actuators A: Physical* 115: 523–529.

Myers R, Vickers M, Kim H, et al. (2007) Small scale windmill. *Journal of Applied Physics* 90: 054106.

Peters DA, Karunamoorthy S and Cao WM (1995) Finite state induced flow models. Part I: two dimensional thin airfoil. *Journal of Aircraft* 32: 313–322.

Pobering S, Ebermeyer S and Schwesinger N (2009) Generation of electrical energy using short piezoelectric cantilevers in flowing media. In: *Proceedings of SPIE 7288*, 728807.

Priya S, Chen CT, Fye D, et al. (2005) Piezoelectric windmill: a novel solution to remote sensing. *Japanese Journal of Applied Physics* 44: L104–L107.

Rancourt D, Tabesh A and Frechette LG (2007) Evaluation of centimeter-scale micro wind mills: aerodynamics and electromagnetic power generation. In: *Proceedings of PowerMEMS 2007*, Freiburg, Germany, pp. 93–96.

Robbins WP, Morris D, Marusic I, et al. (2006) Wind-generated electrical energy using flexible piezoelectric materials. In: *Proceedings of ASME IMECE 2006*, Chicago, Illinois, USA, 5–10 November.

Roundy S and Wright PK (2004) A piezoelectric vibration based generator for wireless electronics. *Smart Materials and Structures* 13: 1131–1144.

Roundy S, Wright PK and Rabaey JM (2003) A study of low level vibrations as a power source for wireless sensor nodes. *Computer Communications* 26: 1131–1144.

Sousa VC, Anicézio MM, De Marqui C Jr, et al. (2011) Enhanced aeroelastic energy harvesting by exploiting

combined nonlinearities: theory and experiment. *Smart Materials and Structures* 20: 094007.

St Clair D, Bibo A, Sennakesavababu VR, et al. (2010) A scalable concept for micropower generation using flow-induced self-excited oscillations. *Applied Physics Letters* 96: 144103.

Tang L, Paidoussis M and Jiang J (2009) Cantilevered flexible plates in axial flow: energy transfer and the concept of flutter-mill. *Journal of Sound and Vibration* 326: 263–276.

Theodorsen T (1935) *General theory of aerodynamic instability and mechanism of flutter*. Langley Memorial Aeronautical Laboratory, NACA-TR-496.

Tvedt LGW, Nguyen DS and Halvorsen E (2010) Nonlinear behavior of an electrostatic energy harvester under wide- and narrowband excitation. *IEEE/ASME Journal of Microelectromechanical Systems* 19: 305–316.

Wagner H (1925) Über die Entstehung des dynamischen Auftriebes von Tragflügeln. *ZAMM: Zeitschrift für Angewandte Mathematik und Mechanik* 5(1): 17–35.

Xu FJ, Yuan FG, Hu JZ, et al. (2010) Design of a miniature wind turbine for powering wireless sensors. In: *Proceedings of SPIE, Sensors and Smart Structures Technologies for Civil, Mechanical, and Aerospace Systems* (ed Tomizuka, Masayoshi), vol. 7647, pp. 764741–764741-9.

Zhu D, Beeby S, Tudor J, et al. (2010) A novel miniature wind generator for wireless sensing applications. In: *Proceedings of IEEE sensors 2010*, Kona, HI, 1–4 November, pp. 1415–1418.